Energy materials

CrossMark

Flexible lignin-derived electrospun carbon nanofiber mats as a highly efficient and binder-free counter electrode for dye-sensitized solar cells

Ying Zhao[1,2] , Yun Liu[3] , Congcong Tong[1,2] , Jing Ru[1,2] , Biyao Geng[1,2] , Zhongqing Ma[1,2] , Hongzhi Liu[1,2,*] , and Likui Wang[3,*]

[1] *School of Engineering, Zhejiang Agriculture and Forestry University, Lin'an District, Hangzhou 311300, Zhejiang Province, China*
[2] *Zhejiang Provincial Collaborative Innovation Center for Bamboo Resources and High-Efficiency Utilization, Lin'an District, Hangzhou 311300, Zhejiang Province, China*
[3] *School of Chemical and Material Engineering, Jiang'nan University, Wuxi 214122, Jiangsu Province, China*

ABSTRACT

A series of flexible carbon nanofiber (CNF) mats have been successfully fabricated via electrospinning of aqueous alkaline lignin-based solutions containing poly (vinyl alcohol) as a spinning-assisted agent, thermal stabilization, and subsequent carbonization at different temperatures. When the carbonization is performed at the temperatures higher than 1000 °C, both graphitizing degree and specific surface area are found to be remarkably enlarged. At the carbonization temperature of 1500 °C, the specific surface area is even as high as 941 m^2 g^{-1}. A series of dye-sensitized solar cells (DSSCs) are then assembled using the as-obtained CNF mats as the binder-free counter electrodes (CEs) and their electrochemical and photovoltaic properties are studied. At carbonization temperature of 1500 °C, the maximum photoelectric conversion efficiency is achieved up to 7.60%, almost equal to that of the DSSCs with a conventional platinum CE (7.67%) as a reference. The excellent photoelectric performance is attributed to the very high specific surface area and low charge transfer resistance of lignin-based CNF mats as a CE. The cost-effective and flexible features make the sustainable CNF mats as a promising alternative CE to replace conventional and expensive platinum for DSSCs.

Introduction

Dye-sensitized solar cells (DSSCs) have attracted considerable interests due to their high-efficiency, low-cost, and relatively high theoretical power conversion efficiency [1, 2]. A typical DSSC device usually is composed of a dye-sensitized nanocrystalline titanium dioxide (TiO_2) photoanode, an electrolyte containing iodide/triiodide (I^-/I_3^-) redox couples, and a counter electrode (CE). Among these components above, CE plays a key role in collecting

🦋 Springer

electrons from external circuit and catalyzing the reduction of the I_3^- species [3, 4]. At present, noble metal platinum (Pt) is the most widely used CE material due to the outstanding electrical conductivity and electrocatalytic activity. However, the high cost and poor anti-corrosive properties in the electrolyte hindered its practical application in the long-term DSSCs device [5–7]. Therefore, numerous efforts have been devoted to the development of cost-effective and electrolyte-resistant CEs to replace Pt.

Recently, various nano-structured carbon materials, such as carbon nanotubes (CNT), graphene, carbon nanofibers (CNFs), and fullerenes, have attracted considerable interests as potential CE materials of DSSCs [8–11]. Dong et al. [12] employed single-walled carbon nanotubes (CNTs) vertically aligned on FTO glass as CEs. The effect of CNTs' length on the electrocatalytic activity was studied, and DSSCs based on CNTs of 34 μm showed a conversion efficiency of 5.5%. Chen et al. [13] obtained carbon nanotube fibers as conductive materials to support dye-loaded TiO₂ nanoparticles in DSSCs. The power conversion efficiency of this nanofiber solar cell can achieve 2.94%. Wu et al. compared the electrochemical catalytic activity of nine kinds of carbon materials that were assembled into DSSCs system as CEs, respectively. The results demonstrate that carbon materials are a promising substitute for the expensive Pt CE for low-cost DSSCs [14]. Huang et al. [15] proposed a drying approach to achieving well distributed and aligned CNT films, and the DSSC based on these films achieved an energy conversion efficiency of 9.05%. Compared to Pt CE, the above nanostructured carbon materials have high electronic conductivity, superior chemical stability, and high reactivity for triiodide reduction [16–20]. Among these nano-structured carbon materials, CNFs have a relatively lower cost and would be a more cost-effective alternative to Pt CEs. Joshi et al. used PAN-based electrospun carbon nanofibers as a low-cost alternative to Pt CE in DSSCs. The carbon nanofibers as a counter electrode exhibited lower performance as that of Pt-based devices [21]. Park et al. [22] prepared hollow carbon nanofibers with mesoporous shell structures through concentric electrospinning, which had a high surface area value of 1191 m² g⁻¹, and the DSSCs based on them had an efficiency of 7.21%, which was comparable to Pt CE. Sebastian et al. [23] synthesized CNFs by the catalytic decomposition of methane, and the electrode characteristic

results evidenced that electrochemical activity of CNFs was mainly controlled by the surface area and surface graphitization. However, the precursors of commercially available CNF are mainly derived from non-renewable fossil-based resources (e.g., polyacrylonitrile) until now; the application of pure biomass-based CNFs in nanofiber-shaped photovoltaic devices is rare. Ma et al. prepared the CNFs derived from alkali lignin and then surface-deposited with Pt nanoparticles. The DSSC based on CNFs–Pt CE exhibited comparable performances to the DSSC based on a conventional Pt CE [24].

Lignin is the second most abundant natural polymer on earth and has been annually produced in a large quantity as an inexpensive by-product in paper pulping and bio-refinery industries. The molecules of lignin contain a large number of aromatic units, thus making it very suitable as a very sustainable and low-cost precursor to prepare CNFs. Electrospinning is a convenient technique for the production of CNFs. Recently, free-standing lignin-derived CNF mats were fabricated through electrospinning followed by carbonization treatment. The resultant CNF mats have demonstrated promising potentials in energy-storage systems, such as electrodes for supercapacitors [25], anode materials for lithium-ion batteries [26, 27], and highly efficient electrocatalyst for oxygen reduction reaction in alkaline fuel cells [28, 29].

In this work, CNF mats were fabricated by electrospinning aqueous solution mixture of alkali lignin and polyvinyl alcohol (PVA) with varying weight ratios and subsequent thermal stabilization at 250 °C, followed by a facile one-step carbonization process. And effects of carbonization temperature on microstructure of the lignin-derived CNF mats were investigated in terms of scanning electron microscopy (SEM), Brunauer–Emmett–Teller (BET) measurement, X-ray diffraction (XRD), and Raman spectrum, respectively. The highest specific surface area as high as 941 m² g⁻¹ was achieved. By the method of preparing larger surface area and the higher graphitization, the CNFs will provide good electron conduction by enhancing the electrode performance. Using the CNF mats as CE materials, the electrochemical and photoelectric properties of DSSCs were examined and the results were compared with a conventional Pt CE. It was found that the maximum photoelectric conversion efficiency was 7.60%, almost equivalent to that of the DSSCs with a Pt CE as a control.

Experimental section

Materials

Alkali lignin with a weight average molecular weight of 10,000 was purchased from Sigma-Aldrich. Poly (vinyl alcohol) (PVA) was purchased from Sigma-Aldrich with molecular weight of 117,000 and hydrolysis degree of 87–89%. Both alkali lignin and PVA were used as received without further purification.

Preparation of lignin/PVA nanofibers via electrospinning

To prepare the spinning dopes with different weight ratios of lignin/PVA (i.e., 50/50, 67/33, 75/25, 80/20), PVA was first dissolved in an appropriate amount of distilled water, and then, the corresponding amounts of lignin were added into aqueous PVA solution (5 wt%) under magnetic stirring at 90 °C. After being cooled to room temperature under stirring, the solution mixture was placed in a 5-mL plastic fitted with a flap-tip 22-G needle and was electrospun using a horizontal electrospinning setup (Yongkang, SS-2535DC). Typically, electrospinning was performed at 15–20 kV with a feeding rate of 1 mL h^{-1}, and the distance from needle tip to plate substrate was set as 20 cm. The composite nanofibers were collected as overlaid mats on the aluminum foil that covered the roller. The lignin/PVA nanofiber mats were finally peeled off from aluminum foils and then stored in a desiccator prior to the use.

Preparation of lignin-based CNFs

The electrospun nanofiber mats were heated at a rate of 5 °C min^{-1} to 250 °C in air and then annealed at this temperature for 1 h. After thermal stabilization, the mats were further heated from 250 °C to the predetermined temperature at a rate of 5 °C min^{-1} under a constant argon flow (300 mL min^{-1}) and then carbonized for 1 h. By varying the carbonization temperature, a series of lignin-derived CNF mats were obtained, respectively. For the convenience of expression, the resultant CNF mat was denoted as 'CNFs-x,' where x represents the used carbonization temperature.

Characterization

A Zeiss Supra 40VP field-emission scanning electron microscope (SEM) was employed to examine the morphologies of nanofiber mats. The average fiber diameter of each sample was determined by measuring diameters of 50 randomly selected nanofibers in the corresponding SEM image using the image-J software. X-ray diffraction (XRD) patterns were acquired from a Rigaku Ultima Plus X-ray diffractometer operated at 40 kV and 90 mA with the CuK$_\alpha$ radiation (wavelength $\lambda = 1.54$ A). Fourier transform infrared (FTIR) spectra were recorded on an IR Prestige-21 infrared spectrometer (Shimadzu, Japan) in the wavenumber range of 4000–400 cm^{-1} at a resolution of 4 cm^{-1} and 32 scans. The thermal stabilities of samples were measured with a TA Instruments Q500 thermogravimetric analyzer (TGA) heating at a rate of 5 °C min^{-1} to 800 °C in N$_2$ atmosphere. Raman spectra were recorded from a Nicolet NXR 9650 FT-Raman spectrometer, and the wavelength of source laser was 632.8 nm. Brunauer–Emmett–Teller (BET) specific surface area, total pore volume, average pore size, and pore size distribution were determined by N$_2$ adsorption at $-$ 196 °C with Micromeritics Analytical Services (Norcross, GA). Elemental analysis (C, H, O, S) was carried out using vario EL cube analyzer (Elementar, Germany). The electrical conductivity tests were performed using a Four Probes tester (RTS-9, Guangzhou Probe) at 10 μA current densities.

Assembling and characterization of the DSSC

TiO$_2$ photoanodes were prepared according to a previously reported method [30]. Typically, the FTO glasses were treated in 40 mM aqueous TiCl$_4$ solution at 70 °C for 30 min and then washed with water and ethanol. TiO$_2$ film consisting of 20 nm TiO$_2$ particles and a light scattering layer composed of 400 nm TiO$_2$ particles were deposited on FTO glass by a screen printing technique, which were sintered by gradually increasing the temperature to 500 °C and kept for 30 min. Then, the TiO$_2$ layers were immersed in 20 mM of TiCl$_4$ aqueous solution at 70 °C for 30 min and then heated at 500 °C for 30 min. After being cooled down to 80 °C, they were put into 0.5 mM N719 dye solution (t-butanol/acetonitrile solution, volume ratio 1:1) for 24 h, followed by

rinsing with copious acetonitrile. The CNF mat was spread onto a FTO glass and used as comparative CE, while Pt-coated FTO glass was used as the working electrode.

The photoanodes and the CEs were assembled together with a 60-μm Surlyn 1702 film. Then, an electrolyte consisting of 0.6 M 1-butyl-3-methyl imidazolium iodide, 0.03 M I_2, 0.10 M guanidinium thiocyanate, and 0.5 M 4-tertbutylpyridine in a mixture of acetonitrile and valeronitrile (volume ratio 85:15) was filled into the cell via a drilled hole, after which the hole was sealed with an adhesive film and glass.

The photovoltaic performance of the DSSC was measured by a digital source meter (Keithley 2440) under an Oriel solar simulator illumination (AM1.5, 100 mW cm^{-2}). The electrochemical impedance spectroscopy (EIS) measurement was carried out on a Zahner Zennium workstation under one-sun illumination under the condition in a three-electrode system in I^-/I_3^- electrolyte by cyclic voltammetry.

Results and discussion

Morphological characteristics

The morphologies of electrospun nanofiber mats prepared from aqueous lignin/PVA solutions with different weight ratios (i.e., 50/50, 67/33, 75/25, and 80/20) were studied using SEM, and the images are shown in Fig. 1. The transition from the mixed bead/nanofiber morphologies to bead-free nanofiber ones was observed as the lignin/PVA ratio was increased. This suggested that a higher lignin content contributed to the formation of perfect nanofibers during the electrospinning. Meanwhile, the electrospun nanofibers from the lignin/PVA (80/20) mixture appeared to become more uniform in diameter. This may be attributed to the enhanced viscosity of electrospun dopes [31]. But with further increasing the lignin/PVA ratio to 85/15, the electrospinning became very difficult to perform smoothly due to the too high viscosity of the lignin/PVA mixture.

After thermal stabilization followed by the carbonization at varying temperatures, these electrospun nanofiber mats can be converted into carbon nanofiber (CNF) ones. From SEM images (Fig. S1), the resulting CNF mats retained nanofibrous morphologies, but the fiber diameter remarkably decreased in comparison with the precursor ones. Furthermore, N_2 adsorption/desorption isotherms of these CNFs obtained at a fixed carbonization temperature of 1500 °C were measured (Fig. S2) and the corresponding performance parameters are outlined in Table S1. The CNF mats prepared from the aqueous lignin/PVA (80/20) solution were found to possess the highest values in both specific surface area and volume ratio of mesopores (Fig. S2). Therefore, on the basis of the aforesaid findings, 80/20 (w/w) was chosen as the optimal operating ratio of lignin/PVA to prepare CNFs in the subsequent investigation.

Figure 2 presents SEM images of the CNF mats prepared from an aqueous lignin/PVA (80/20, w/w) mixture but different carbonization temperatures. One can note that all the CNFs retained fibrous morphologies after the carbonization but some broken nanofibers were visible. The average diameters of CNFs were determined, and the results are listed in Table 1. Compared to the precursor ones (Fig. 1d), these CNFs appeared finer. With elevating carbonization temperature, the lateral size of CNFs gradually became smaller, as one generally expected. In the case of the 'CNFs-1500' sample, the average diameter of nanofibers was as low as 200 nm, which was comparable to the previously reported result [32]. Notably, many nano-cavities were also observed on the surfaces of the 'CNFs-1500' one (see the insert in Fig. 3d).

It is known that carbonization temperature has a significant effect on structure and properties of CNFs [33]. To ensure that naturally occurring lignin as the char-forming component that formed the rich phase, the electrospun lignin/PVA nanofibers with a weight ratio of 80/20 were chosen as the precursor of carbon nanofibers to further investigate the impacts of carbonization temperature on microstructure of the as-obtained CNFs. In our preliminary work, it was found that the pre-stabilizing treatment of the nanofiber precursor in air prior to carbonization was essential to improve the yield of as-obtained CNF mats. In this work, a further increase in carbonization temperature above 1500 °C was not further performed since this would result in a remarkable decrease in the yield of lignin-derived CNF mats. In our work, the as-obtained free-standing CNF mats exhibited good flexibility, which was demonstrated by repeated folding or bending for 50 cycles without failure (see Fig. 3). Thus, this advantage made it favorable for the use of flexible counter electrodes of DSSCs.
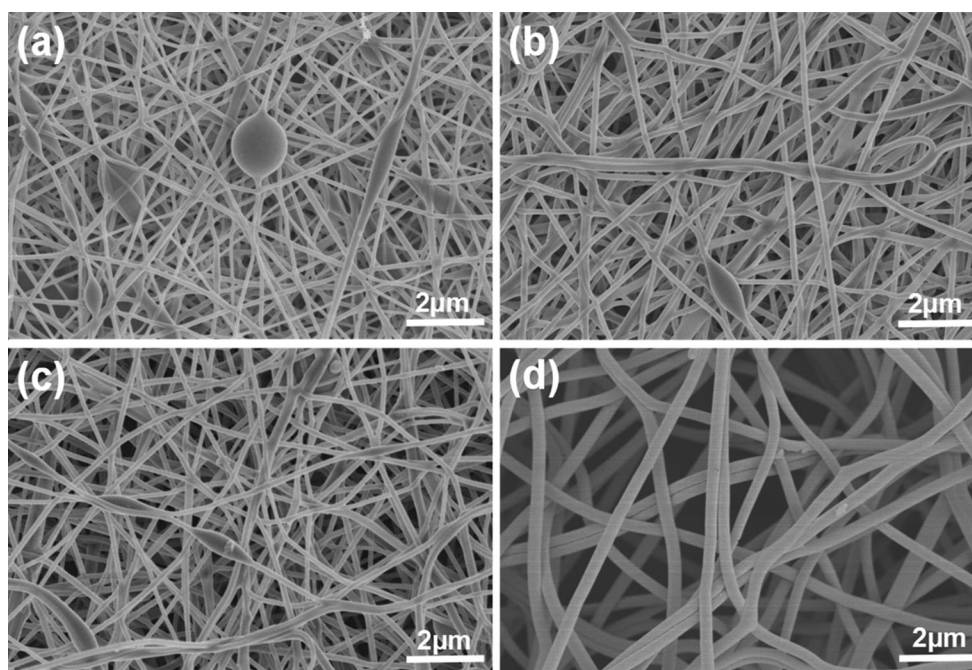
Figure 1 SEM images of electrospun nanofibers from aqueous lignin/PVA solutions with varying weight ratios of lignin/PVA: **a** 50/50, **b** 67/33, **c** 75/25, **d** 80/20.
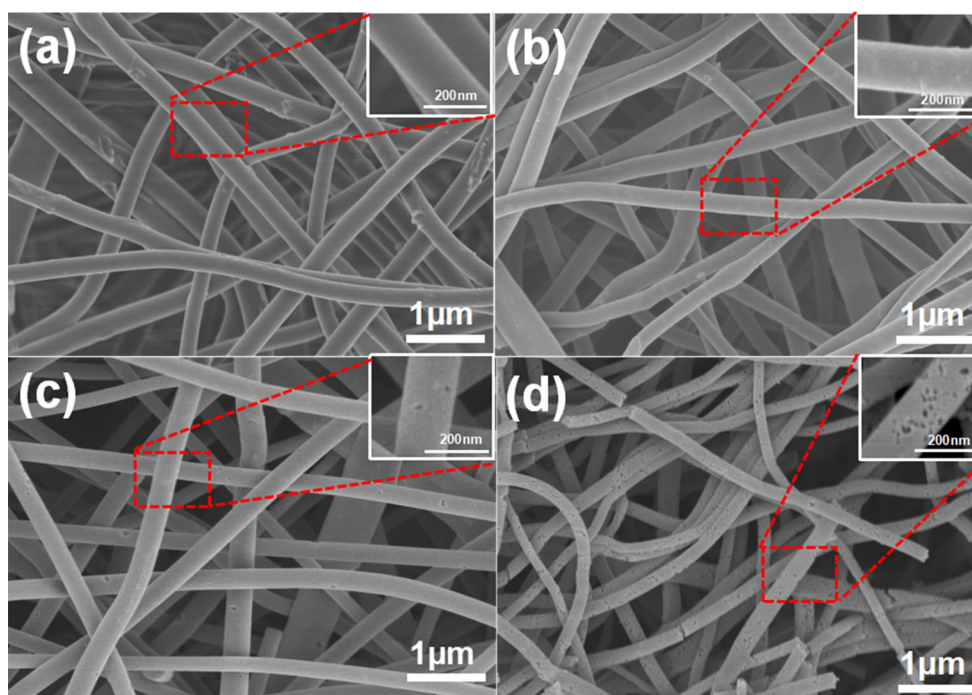

Figure 2 SEM images of CNFs prepared from a fixed lignin/PVA mixture ratio at 80/20 and varying carbonization temperatures: **a** 800 °C, **b** 1000 °C, **c** 1200 °C, **d** 1500 °C.

The effect of carbonization temperature on chemical structure of lignin-derived CNFs was revealed by Fourier transformed infrared (FTIR) spectra. As shown in Fig. 4, the main adsorption peaks of functional groups, such as O–H stretching ($\upsilon \sim 3420$ cm^{-1}), C–H stretching ($\upsilon \sim 2921$ cm^{-1}),

Table 1 Structural characteristics of CNF mats prepared at different carbonization temperatures

Samples	Average diameters (nm)	BET surface area ($m^2\ g^{-1}$)	Pore size (nm)	Total pore volume, V_{total} ($cm^3\ g^{-1}$)	Pore volume of mesopore ($cm^3\ g^{-1}$)	I_D/I_G	Electric conductivity ($S\ m^{-1}$)
CNFs-800	253 ± 11	193	2.53	0.12	0.02	1.34	81
CNFs-1000	236 ± 18	272	2.44	0.17	0.05	1.12	212
CNFs-1200	225 ± 22	773	2.25	0.43	0.22	1.05	496
CNFs-1500	200 ± 20	941	2.19	0.53	0.30	0.97	502

Figure 3 Flexibility display pictures of lignin-derived CNF mats.
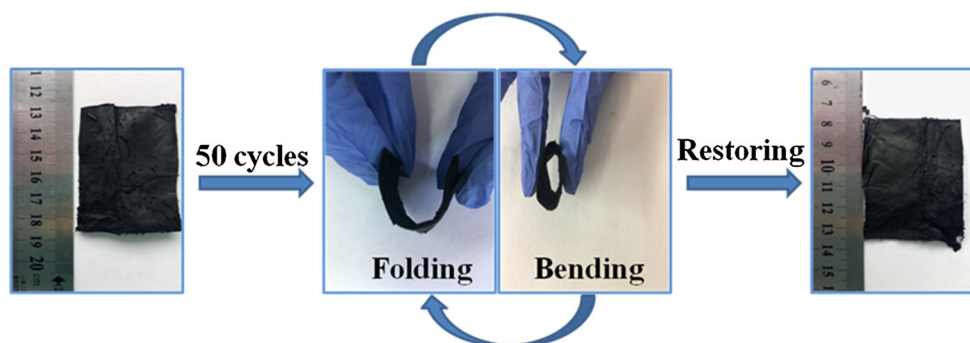
C=O stretching ($\upsilon \sim 1738\ cm^{-1}$), C–H bending ($\delta \sim 1370\ cm^{-1}$), and C–O stretching ($\upsilon \sim 1242\ cm^{-1}$), gradually became less intense and finally disappeared. This result indicated that an increase in pyrolysis temperature contributed to the consistent improvement of carbonization degree.

The crystalline structures of CNF mats were investigated by XRD and Raman spectroscopy analysis. Figure 5a shows XRD patterns of lignin-derived CNFs prepared at different carbonization temperatures. When carbonization temperature exceeded
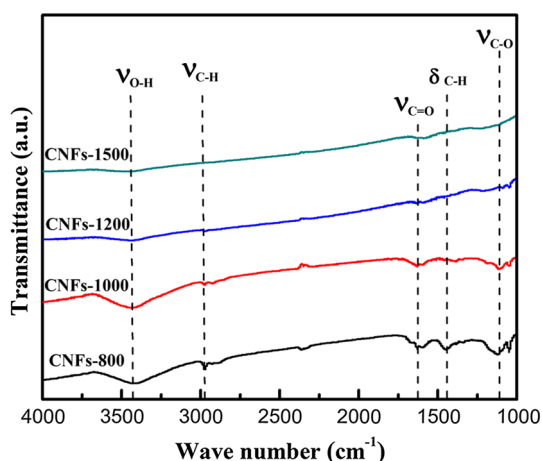
Figure 4 FTIR spectra of CNF mats prepared at different carbonization temperatures.

1000 °C, both diffraction peaks centered at 2θ angles of 24.6° and 44° were perceptible, which were attributed to the crystallographic planes of (002) and (101) in the graphitic structure, respectively [34]. Moreover, with increasing CNFs carbonization temperature from 1200 to 1500 °C, the diffraction peaks became more intense and slightly shifted toward a higher diffraction angle, which suggested an increased degree of graphitization in the CNFs. But the broadening nature of these two peaks indicated still relatively low degree of graphitization [35]. However, in the case of the mat samples carbonized at the lower temperatures (i.e., CNFs-800 and CNFs-1000), there existed several relatively sharp peaks located at 2θ angles of 26°, 33°, and 34°, whose origin of their crystallographic structure was unclear.

Compared with XRD, Raman spectroscopic technique is more sensitive to structural changes of disordered carbons [36]. Figure 5b further shows Raman spectra for lignin-derived CNF mats prepared at different carbonization temperatures. Two characteristic bands around 1350 and 1580 cm^{-1} were present for all the samples. The one at 1580 cm^{-1} was attributed to the graphite (G) band, and the other at 1350 cm^{-1} was related to the disorder carbon (D). The intensity ratio of 'D-band' to 'G-band' ('I_D/I_G,' also known as the 'R-value') indicated the degree of

Figure 5 XRD (**a**) and Raman (**b**) spectra of CNF mats prepared at different carbonization temperatures.
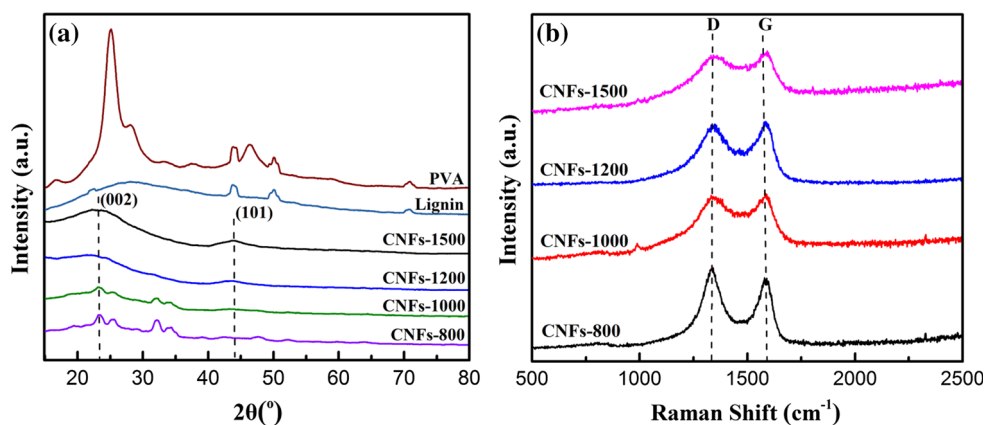
structural order in carbonaceous materials [37]. With increasing carbonization temperatures from 800 to 1500 °C, the *R*-value of CNF mat samples monotonically decreased from 1.34 to 0.97 (Table 1), suggesting that some disordered carbonaceous structures were gradually converted to ordered graphitic ones with increasing carbonization temperature. This result was further supported by the measured electric conductivity order of these lignin-derived CNF mats, in which the higher carbonization temperature, the higher electric conductivity (Table S1).

In order to clarify the origin of the sharp crystallographic peaks in Fig. 5, thermogravimetric analysis of pure alkali lignin and PVA under nitrogen was further investigated and their TGA curves are given in Fig. 6. When being heated to 900 °C, PVA almost completely decomposed, whereas the weight residue left by alkali lignin still remained at a level of about 47%. Therefore, the sharp diffraction peaks for the CNFs-800 and CNFs-1000 mat samples could originate from some crystalline intermediate produced during the carbonization of alkaline lignin. This result also indicated that lignin rather than PVA was the char-forming component of the CNF mats, whereas PVA component only acted as a spinning-assisted agent in our work.

Table 2 Element contents of the CNFs prepared at different carbonization temperatures

Samples	Element content (wt%)			
	C	H	O	S
CNFs-800	42.2	18.3	32.7	5.7
CNFs-1000	57.7	9.1	27.5	5.7
CNFs-1200	58.2	13.1	24.4	4.3
CNFs-1500	81.3	4.8	12.1	1.8

The specific surface area and porous structures of CNF mats were also studied by N_2 adsorption–desorption analysis in Fig. 7. All the isotherms of CNF mat samples showed a typical type-IV isotherm with a N_2 hysteresis loop, indicating mesoporous structure [38]. The characteristics of their porous structure are outlined in Table 1. With increasing carbonization temperature, both BET specific surface area and total pore volume (V_{tot}) values of lignin-derived CNFs increased gradually and a sharp increase was observed after 1000 °C. The specific surface area and V_{tot} of CNFs-1500 reached the maximum, respectively, that is 941 m^2 g^{-1} and 0.53 cm^3 g^{-1}. Notably, the ratio of mesopore to the total pore volume progressively increased when carbonization temperature was increased from 800 to 1500 °C. Especially for CNFs-1000 to CNFs-1500 samples, the mesoporous structure was well developed. For instance, the mesopores contributed to only 17% of the total pore volume for the CNFs-800, whereas the contribution of mesopores became dominant at carbonization temperature higher than 1000 °C. And the volume ratio of mesopore reached 51% for the CNF-1200 and 57% for the CNF-1500, respectively.

To recall the aforesaid SEM observation in Fig. 2d, a large number of nano-pores with the size in 30 ± 10 nm are noted on the surfaces of lignin-derived CNFs prepared at 1500 °C. And elemental analysis results (Table 2) showed that an increase in carbonization temperature yielded a dramatic decrease in the contents of non-carbon atoms (i.e., sulfur, oxygen, and hydrogen). For the 'CNF-1500' sample, the weight contents of sulfur, oxygen, and hydrogen elements were only 1.8, 12.1, and 4.8%, respectively, while 5.7, 32.7, and 12.3% were for the 'CNF-800' one. Thus, the meso-sized pores in the

CNFs-1500 sample were presumably caused by the removal of massive hydrogen, oxygen, and sulfur elements at such a high carbonization temperature, thereby resulting in the highest specific surface area.

Photovoltaic performance of the CNF

The photovoltaic performances of the DSSCs with CNF mats as CEs are shown in Fig. 8, and the detailed photovoltaic characteristics are outlined in Table 3. The conversion efficiency of the cell with the CNF mat carbonized at 800 °C was 5.83% with a short-circuit current density of 12 mA cm^{-2}. With an increase in carbonization temperature to 1000, 1200, and 1500 °C, the short-circuit current density was increased to 13.63, 15.54, 15.94 mA cm^{-2}, respectively, while the conversion efficiency was 6.90% for 1000 °C, 7.46% for 1200 °C, and 7.60% for 1500 °C. It was evident from the data that the increasing carbonization temperature resulted in an improvement in both short-circuit current density and conversion efficiency. This could be contributed to both higher graphitization degree and larger specific surface area caused by carbonization at the higher temperature. The performance of the DSSC based on CNF mat carbonized at 1500 °C was quite close to that of the DSSC based on Pt electrode (7.67%) [39]. These results indicated that the cost-effective lignin-derived CNF mat proposed in this work might be a very promising alternative to expensive Pt electrodes [40].

The electrochemical properties of the DSSC with different CEs were further studied by EIS analysis, and the resulted Nyquist diagrams are shown in Fig. 9. In the equivalent circuit, R_{ct1} represented the electron transfer resistance at the CE and R_{ct2} was mainly attributed to the charge transfer process at the TiO$_2$/dye/electrolyte interface. R_s reflected the sheet resistance mainly dominated by the FTO/glass substrate [41]. The values of R_s, R_{ct1}, R_{ct2} were fitted using the ZView software and are listed in Table 4.

Table 4 Fitting parameters extracted from the Nyquist plots of the DSSCs with different CEs

Samples	R_s (Ω cm^2)	R_{ct1} (Ω cm^2)	R_{ct2} (Ω cm^2)
Pt control	3.57	1.66	11.82
CNFs-800	5.20	27.44	61.64
CNFs-1000	2.97	3.91	34.60
CNFs-1200	3.27	1.97	17.66
CNFs-1500	2.77	1.79	14.58

For the DSSC based on CNF-800 mat, the R_{ct1} value was 27.44 Ω cm^2, and with the increase in the carbonization temperature to 1000, 1200, and 1500 °C, the R_{ct1} decreases to 3.91, 1.97, and 1.79 Ω cm^2, respectively. This suggested that the carbonization at higher temperature would improve the catalytic properties of the CNF mats. Electron supply from CE also influences R_{ct2} [42], which decreases with the increase in the carbonization temperature as well. The R_{ct1} and R_{ct2} of the DSSC based on the CNFs-1500 mat were slightly larger than those of the DSSC based on Pt electrode, which accounted for the superior photovoltaic performance of the Pt electrode. The EIS test results were well in correspondence with the photovoltaic performance of the cells.

Table S1 summarizes performance comparison of CNF-based counter electrodes derived from different carbon sources. The electrospinning of polymer solutions followed by carbonization was also more advantageous in morphological manipulation of CNFs than direct carbonization or high-temperature pyrolysis [13, 23, 44]. As compared to the CNFs prepared from petroleum-based polymers such as polyacrylonitrile [21] and polyaniline [25, 43, 44], the CNF mats prepared using naturally derived and abundant lignin as a carbon source appeared to be more cost-effective and environmentally friendly. Unlike the previously reported lignin-derived CEs [24], the as-prepared lignin-based CNF mats in our work were metal-free and moreover exhibited almost

Table 3 Photovoltaic parameters of DSSCs with different CEs

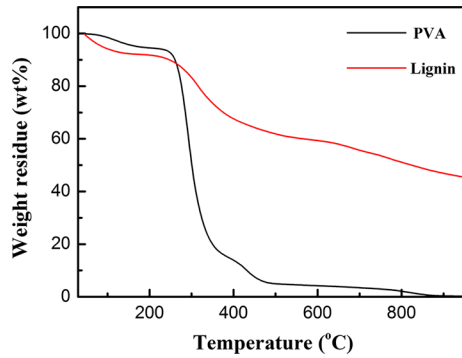| Samples	V_{oc} (V)	J_{sc} (mA cm^{-2})	V_{max} (V)	J_{max} (mA cm^{-2})	FF	PCE (%)
Pt	0.74	16.61	0.53	14.57	0.63	7.67
CNFs-800	0.71	12.00	0.57	10.27	0.68	5.83
CNFs-1000	0.71	13.63	0.57	12	0.71	6.90
CNFs-1200	0.64	15.54	0.52	14.31	0.75	7.46
CNFs-1500	0.65	15.94	0.52	14.53	0.73	7.60

Figure 6 TGA curves of pure alkaline lignin and PVA in N_2.

comparable energy conversion efficiency to commonly used Pt CEs when being assembled into DSSCs [43, 45]. Besides, the free-standing and mechanically flexible advantages would enable it to have a promising potential for the use of flexible CEs in the DSSC devices.

Conclusions

In summary, the flexible and biomass-derived CNF mats were prepared by the carbonization of the electrospun fibers from aqueous lignin/PVA mixture at different temperatures. The morphologies and properties of CNF mats were studied with SEM, BET, XRD, and Raman spectra. With elevating carbonization temperature, the degree of graphitization and specific surface area of the mats gradually increased. When the carbonization was performed at 1500 °C, the largest specific surface area as high as 941 m^2 g^{-1} was obtained, which was the highest value for the ever-reported lignin-derived CNF mats to the best of our knowledge. The CNF mats obtained at different temperatures were employed as binder-free counter
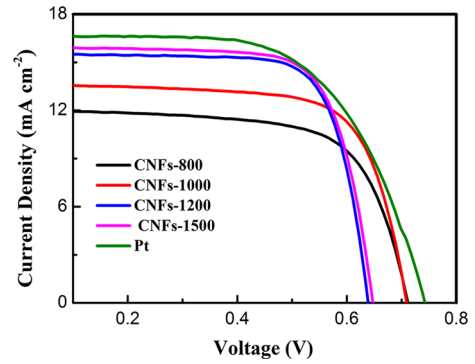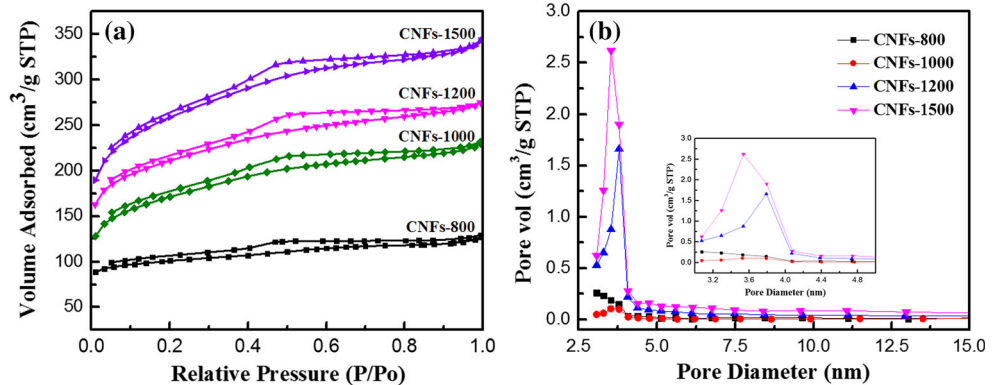

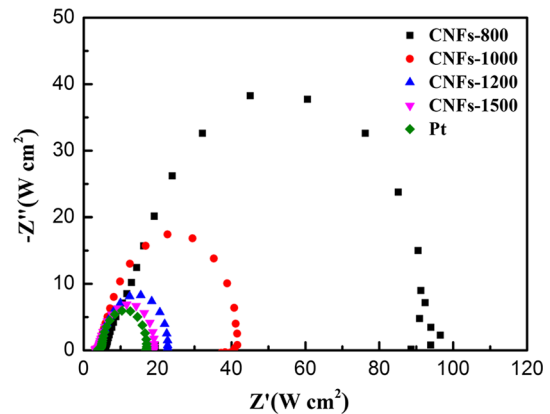**Figure 8** J–V curves for the DSSC with different CEs at different temperatures.

Figure 9 Nyquist plots of EIS of DSSCs measured at open-circuit voltage (VOC) from 100 kHz to 0.1 Hz under 1-sun illumination.

electrodes (CEs) of DSSCs as an alternative to expensive Pt. The photovoltaic conversion efficiency of the DSSCs depended largely on carbonization temperatures, at which the lignin-derived CEs were prepared. For the DSSC based on CNF mats obtained at 1500 °C, a conversion efficiency of 7.60% was achieved, quite close to the counterpart of Pt-based

Figure 7 N_2 adsorption/desorption isotherms (**a**) and pore size distribution curves (**b**) of different lignin-derived CNFs.

DSSCs (7.67%) as a control. This work suggested that the flexible CNF mats derived from lignin would be a promising cost-effective alternative to the expensive Pt CE.

Acknowledgements

Electronic supplementary material: The online version of this article (https://doi.org/10.1007/s10853-018-2059-0) contains supplementary material, which is available to authorized users.

References

[1] Regan BO, Gratzel M (1991) A low-cost, high-efficiency solar cell based on dye-sensitized colloidal TiO$_2$ films. Nature 353:737–740

[2] Papageorgiou N (2004) Counter-electrode function in nanocrystalline photoelectrochemical cell configurations. Coord Chem Rev 248:1421–1446

[3] Li GR, Wang F, Jiang QW et al (2010) Carbon nanotubes with titanium nitride as a low-coat counter electrode material for dye-sensitized solar cells. Angew Chem Int Ed 122:3653–3656

[4] Hou Y, Chen ZP, Wang D et al (2014) Highly electrocatalytic activity of RuO$_2$ nanocrystals for triiodide reduction in dye-sensitized solar cells. Small 10:484–492

[5] Kubo D, Tadanaga K, Hayashi A et al (2013) Improvement of electro-chemical performance in alkaline fuel cell by hydroxide ion conducting Ni–Al layered double hydroxide. J Power Sour 222:493–497

[6] Zhao W, Zhu X, Bi H et al (2013) Novel two-step synthesis of NiS nanoplatelet arrays as efficient counter electrodes for dye-sensitized solar cells. J Power Sour 242:28–32

[7] Wu J, Gross A, Yang H (2011) Shape and composition-controlled platinum alloy nanocrystals using carbon monoxide as reducing agent. Nano Lett 11:798–802

[8] Zhao AQ, Masa J, Muhler M et al (2013) N-doped carbon synthesized from N-containing polymers as metal-free catalysts for the oxygen reduction under alkaline conditions. Electrochim Acta 98:139–145

[9] Huang QH, Tao L, Qiao SZ et al (2013) Pyrite nanorod arrays as an efficient counter electrode for dye-sensitized solar cells. J Mater Chem A 1:11828–11833

[10] Zhang J, Fang J (2009) A general strategy for preparation of Pt 3d-transition metal (Co Fe, Ni) nanocubes. J Am Chem Soc 131:18543–18547

[11] Kang Y, Murray CB (2010) Synthesis and electrocatalytic properties of cubic Mn–Pt nanocrystals (nanocubes). J Am Chem Soc 132:7568–7572

[12] Dong P, Pint CL, Hainey M et al (2011) Vertically aligned single-walled carbon nanotubes as low-cost and high electrocatalytic counter electrode for dye-sensitized solar cells. ACS Appl Mater Interfaces 3:3157–3161

[13] Chen T, Qiu LB, Cai ZB et al (2012) Intertwined aligned carbon nanotube fiber based dye-sensitized solar cells. Nano Lett 215:2568–2572

[14] Wu M, Lin X, Wang T et al (2011) Low-cost dye-sensitized solar cell based on nine kinds of carbon counter electrodes. Energy Environ Sci 4:2308–2315

[15] Huang S, Yang Z, Zhang L et al (2012) A novel fabrication of a well distributed and aligned carbon nanotube film electrode for dye-sensitized solar cells. J Mater Chem 22:16833–16838

[16] Hagfeldt A, Boschloo G, Sun L et al (2010) Dye-sensitized solar cells. Chem Rev 110:6595–6663

[17] Theerthagiri J, Senthil AR, Madhavan J et al (2015) Recent progress in non-platinum counter electrode materials for dye-sensitized solar cells. Chemelectrochem 2:928–945

[18] Kouhnavard M, Ludin NA, Ghaffari BV (2015) Carbonaceous materials and their advances as a counter electrode in dye-sensitized solar cells: challenges and prospects. Chemsuschem 8:1510–1533

[19] Zhou Y, Yang M, Wu W et al (2015) Room-temperature crystallization of hybrid-perovskite thin films via solvent–solvent extraction for high-performance solar cells. J Mater Chem A 3:8178–8184

[20] Poudel P, Qiao Q (2014) Carbon nanostructure counter electrodes for low cost and stable dye-sensitized solar cells. Nano Energy 4:157–175

[21] Joshi P, Zhang L, Chen Q et al (2010) Eletrospun carbon nanofibers as low-cost counter electrode for dye-sensitized solar cells. ACS Appl Mater Interfaces 2:3572–3577

[22] Park SH, Kim BK, Lee W (2013) Electrospun activated carbon nanofibers with hollow core/highly mesoporous shell structure as counter electrodes for dye-sensitized solar cells. J Power Sour 239:122–127

[23] Sebastian D, Baglio V, Girolamo M (2014) Carbon nanofiber-based counter electrodes low cost dye-sensitized solar cells. J Power Sour 250:242–249

[24] Ma XJ, Elbohy H, Sigdel S et al (2016) Electrospun carbon nano-felt derived from alkali lignin for cost-effective counter electrodes of dye-sensitized solar cells. RSC Adv 6:11481–11487

[25] Wang R, Wu QD, Lu Y et al (2014) Preparation of nitrogen-doped TiO_2/graphene nanohybrids and application as counter electrode for dye-sensitized solar cells. ACS Appl Mater Interfaces 6:2118–2124

[26] Wang SX, Yang LP, Stubbs LP et al (2013) Lignin-derived fused electrospun carbon fibrous mats as high performance anode materials for lithium ion batteries. ACS Appl Mater Interfaces 5:12275–12282

[27] Lai CL, Zhou ZP, Zhang LF et al (2014) Free-standing and mechanically flexible mats consisting of electrospun carbon nanofibers made from a natural product of alkali lignin as binder-free electrodes for high-performance supercapacitors. J Power Sour 247:134–141

[28] Ma XJ, Kolla P, Zhao Y et al (2016) Electrospun lignin-derived carbon nanofiber mats surface-decorated with MnO_2 nanowhiskers as binder-free supercapacitor electrodes with high performace. J Power Sour 325:541–548

[29] Greiner A, Wendorff JH (2007) Electrospinning: a fascinating method for the preparation of ultrathin fibres. Angew Chem Int Ed 46:5670–5703

[30] He B, Tang Q, Luo J et al (2014) Rapid charge-transfer in polypyrrole–single wall carbon nanotube complex counter electrodes: improved photovoltaic performances of dye-sensitized solar cells. J Power Sour 256:170–177

[31] Wu Y, Cai S, Wang D et al (2012) Syntheses of water-soluble octahedral, truncated octahedral, and cubic Pt–Ni nanocrystals and their structure-activity study in model hydrogenation reactions. J Am Chem Soc 134:8975–8981

[32] Ito S, Murakami TN, Comte P et al (2008) Fabrication of thin film dye sensitized solar cells with solar to electric power conversion efficiency over 10%. Thin Solid Films 516:4613–4619

[33] Choi DI, Lee JN, Song JC et al (2013) Fabrication of polyacrylonitrile/lignin-based carbon nanofibers for high-power lithium ion battery anodes. J Solid State Electrochem 17:2471–2475

[34] Schreiber M, Vivekanandhan S, Mohanty AK et al (2015) Iodine treatment of lignin-cellulose acetate electrospun fibers: enhancement of green fiber carbonization. ACS Sustain Chem Eng 3:33–41

[35] Qiu H, Huang X (2012) Retracted article: nanoporous PtFe surface alloy architecture for enhanced methanol electro-oxidation. J Mater Chem 22:7602–7608

[36] Dao VD, Choi HS (2013) An optimum morphology of platinum nanoparticles with excellent electrocatalytic activity for a highly efficient dye-sensitized solar cell. Electrochim Acta 93:287–292

[37] Barakat NAM, Motlak M, Elzatahry AA (2014) Ni_xCo_{1-x} alloy nanoparticle-doped carbon nanofibers as effective non-precious catalyst for ethanol oxidation. Int J Hydrog Energy 39:305–316

[38] Chen C, Kang Y, Huo Z et al (2014) Highly crystalline multimetallic nanoframes with three-dimensional electrocatalytic surfaces. Science 343:1339–1343

[39] Nassr AB, Sinev I, Pohl MM (2014) Rapid microwave-assisted polyol reduction for the preparation of highly active PtNi/CNT electrocatalysts for methanol oxidation. ACS Catal 4:2449–2462

[40] Han J, Kim H, Kim DY et al (2010) Water-soluble polyelectrolyte-grafted multiwalled carbon nanotube thin films for efficient counter electrode of dye-sensitized solar cells. ACS Nano 4:3503–3509

[41] Guo F, Cao DX, Du MM et al (2016) Enhancement of direct urea-hydrogen peroxide fuel cell performance by three-dimensional porous nickel-cobalt anode. J Power Sour 307:697–704

[42] Ago M, Okajima K, Jakes JE et al (2012) Lignin-based electrospun nanofibers reinforced with cellulose nanocrystals. Biomacromol 13:918–926

[43] Veerappan G, Kwon W, Rhee SW (2011) Carbon-nanofiber counter electrode for quasi-solid state dye-sensitized solar cells. J Power Sour 196:10798–10805

[44] Chen JZ, Li B, Zheng JF, Zhao JH, Jing HW, Zhu ZP (2011) Polyanilinenanofiber/carbon film as flexible counter electrodes in platinum-free dye-sensitized solar cells. Electrochim Acta 56:4624–4630

[45] He JX, Zhou MJ, Wang LD, Zhao SY, Wang Q, Ding B, Cui SZ (2016) Electrospinning in situ synthesis of graphene-doped porous copper indium disulfide/carbon composite nanofibers for highly efficient counter electrode in dye-sensitized solar cells. Eletrochim Acta 215:626–636